KSME

Springer

Journal of Mechanical Science and Technology 35 (10) 2021

Original Article
DOI 10.1007/s12206-021-09019

Compound fault diagnosis and identification of hoist spindle device based on hilbert huang and energy entropy

Jun Gu[1], Yuxing Peng[1,2], Hao Lu[1,2], Bobo Cao[1] and Guoan Chen[3]

[1]School of Mechatronic Engineering, China University of Mining and Technology, Xuzhou, China, [2]Jiangsu Key Laboratory of Mine Mechanical and Electrical Equipment, China University of Mining and Technology, Xuzhou, China, [3]The Army Engineering University Training Base of PLA, Xuzhou, China

Keywords:
· Energy entropy
· Fault diagnosis
· Filter
· Hilbert-Huang transform
· Hoist
· Spindle device

Correspondence to:
Jun Gu
gujuncumt@163.com

Citation:
Gu, J., Peng, Y., Lu, H., Cao, B., Chen, G. (2021). Compound fault diagnosis and identification of hoist spindle device based on hilbert huang and energy entropy. Journal of Mechanical Science and Technology 35 (10) (2021) 4281~4290. http://doi.org/10.1007/s12206-021-09019

Received May 16th, 2020
Revised January 28th, 2021
Accepted July 4th, 2021

† Recommended by Editor No-cheol Park

Abstract Aiming at the complex fault signal components and difficulty in identifying the fault features of a hoist spindle device, this study proposes a method based on a filtering algorithm, Hilbert-Huang transform (HHT), energy entropy, and support vector machines (SVM). The filtering method is applied to the vibration signal under different fault conditions. Then, the Hilbert-Huang transform is applied to the noise-reduced signal. The empirical mode decomposition (EMD) method decomposes the noise-reduced vibration signal into a set of intrinsic mode functions (IMF). Then, the Hilbert transform (HT) calculates the envelope spectrum of the first few IMFs. Afterward, it evaluates and extracts the fault characteristic frequencies. Finally, the identification of different fault defect types is determined by combining the intrinsic modal energy entropy and SVM. The experimental results show that the method can accurately identify the faults in the rotor bearing system and is an effective fault signal processing method.

1. Introduction

As the “throat” of the mine, a hoist is used to drive minerals, personnel, and important equipment by winding wire ropes [1, 2]. A series of mechanical failures inevitably occur in the bearing and the spindle of the spindle device. The rolling bearing can experience failure, which can be divided into an outer ring fault, an inner ring fault, a rolling element fault, and a comprehensive situation. In addition, the failure types of the main shaft can be divided into misalignment, bending, cracking, rubbing, loosening, and the like. The probability of a compound fault in a spindle device is higher than that of a single fault. However, few studies have discussed compound faults.

The fault diagnosis method based on vibration analysis is generally divided into three stages. The first stage is the vibration signal data acquisition. The second stage is signal processing, which can be divided into three types: time domain analysis [3], frequency domain analysis [4], and time-frequency domain analysis. In the last stage, the statistical features are extracted from the time domain, frequency domain, and time-frequency domain to obtain useful information. Time domain analysis is the simplest and most intuitive image. Frequency domain analysis methods typically diagnose mechanical faults by observing the frequency of fault characteristics in the vibration signal. For the non-stationary signal of mechanical vibration, several time-frequency analysis techniques are introduced for fault diagnosis [5], such as wavelet transform (WT), short-time Fourier transform (STFT) [6], Wigner-Ville distribution (WD), and Choi-Williams distribution (CWD). These methods cannot adaptively decompose signals in the time-frequency domain.

For example, the WT is known as the “mathematical microscope,” which can provide localized information in the time domain and frequency domain. Many scholars have used it in the

time-frequency analysis of vibration signals. However, WT also has some problems. For instance, the selection of a basis function will influence the effect of the wavelet analysis. Meanwhile, the disadvantage of STFT is that the window size for all frequencies is fixed [7, 8].

Empirical mode decomposition (EMD), which is an adaptive method for time-frequency analysis proposed by Huang [9], can decompose the signal into a series of intrinsic mode functions (IMF) with different characteristic scales [10]. The EMD method has a wide range of applications in the diagnosis of rotor-bearing mechanical faults [11, 12]. Ming et al. [13] used the Hilbert envelope iterative calculation to separate the deterministic signal components in the signal gradually, eliminate frequency shift and DC offset, and extract fault features. Lei et al. [14] summarized the application of EMD in the fault diagnosis of rotating machinery from the perspective of rolling bearing, gear, rotor, and other key components.

Aiming at the problem on the difficulty to demodulate the fault information of the spindle device, the EMD and Hilbert envelope analysis are combined and applied to fault signal processing.

Support vector machine (SVM), proposed by Cortes and Vapnik [15], is an intelligent fault pattern recognition method developed on the basis of statistical learning theory. It adopts the principle of structural risk minimization and shows excellent characteristics in solving problems, such as small sample, nonlinear pattern, and high-dimensional pattern recognition [16, 17].

In this study, filter algorithm, Hilbert-Huang transform (HHT), energy entropy, and SVM are applied to the diagnosis and identification of a spindle-bearing compound fault. The structure of the rest of this paper is as follows. Sec. 2 introduces the basic analysis theory of EMD, Hilbert transform (HT), filtering algorithm, and energy entropy. The third section introduces the process of the method. The test equipment is introduced in Sec. 4. Then, the experimental results and discussion are sorted out in Sec. 5. Finally, the conclusion is drawn in Sec. 6.

2. Theoretical background

2.1 Hilbert-Huang transform

HHT includes empirical mode decomposition and HT.

The decomposition process of EMD is similar to the process of "screening." The specific decomposition process can be viewed in Refs. [18-20].

For the intrinsic modal function $c_i(t)$, we can always have its Hilbert transformation as [21, 22]

$$H\left[c_i(t)\right]=\frac{1}{\pi}\int_{-\infty}^{\infty}\frac{c_i(t')}{t-t'}dt' . \tag{1}$$

By this definition, we can obtain an analytic signal

$$z_i(t)=c_i(t)+jH\left[c_i(t)\right]=a_i(t)e^{j\varphi_i(t)} \tag{2}$$

where amplitude $a_i(t)$ is

$$a_i(t)=\sqrt{c_i^2(t)+H^2\left[c_i(t)\right]} . \tag{3}$$

At this point, the Hilbert envelope spectrum of $c_i(t)$ can be obtained by applying fast Fourier transform to the amplitude of the analytic signal $a_i(t)$.

2.2 Intrinsic modal energy entropy

The energy of each IMF is calculated as $E_1, E_2, E_3, \ldots E_n$, which represents the energy distribution of signals in different frequency bands. According to this calculation, the modal energy entropy is defined as follows [23, 24]:

$$H_{EN}=-\sum_{i=1}^{n}p_i\log p_i \tag{4}$$

where $p_i=E_i/E$ represents the proportion of the energy of the ith IMF in the total energy. H_{EN} stands for energy entropy. According to the energy entropy value, the working state of the spindle device can be assessed.

2.3 Theoretical analysis of filtering algorithm

2.3.1 Noise reduction deviation mean square error

For the $x(t)$ of the vibration signal containing noise, after being decomposed by EMD, the low pass filter can be designed to

$$LP_k=\sum_{i=k}^{n}IMF_i(t)+r_n(t) . \tag{5}$$

Meanwhile, the high pass filter can be expressed as

$$HP_p=\sum_{i=1}^{p}IMF_i(t) . \tag{6}$$

Similarly, the band pass filter can be expressed as

$$BP_b^q=\sum_{i=b}^{q}IMF_i(t) \tag{7}$$

where p and q are the upper truncation parameters of the filter; k and b are the lower truncation parameters of the filter.

Defining the noise reduction deviation mean square error MSE_f of any algorithm f is

$$MSE_f=\sqrt{\frac{\sum_{j=1}^{m}\left(y_j-x_j\right)^2}{m}} \tag{8}$$

where x_j is the value of the noisy signal, m is the total number of sampled signals, y_j is the result of noise reduction, and $j=1,2,\ldots m$.

2.3.2 Filter smoothness

If the two curves $P(t)$ and $Q(t)$ $(0 \le t \le 1)$ reach the same curvature at the combined point $P(1)$ or $Q(0)$,

$$K_{p(1)} = \frac{\left|P''(1)\right|}{\left[1+P'(1)\right]^{3/2}} = \frac{\left|Q''(0)\right|}{\left[1+Q'(0)\right]^{3/2}} = K_{Q(0)}, \tag{9}$$

$$P''(1) \approx \frac{P(1-2h)-2P(1-h)+P(1)}{h^2}, \tag{10}$$

$$Q''(0) \approx \frac{Q(0+2h)-2Q(0+h)+Q(0)}{h^2}. \tag{11}$$

The smoothness of the filter curve $f(x)$ at a point x_0 can be obtained as [25]:

$$SN\big|_{x=x_0} = f(x_0+2h)-f(x_0-2h)- 2\left[f(x_0+h)-f(x_0-h)\right] \tag{12}$$

where h is the sampling step size.

The smoothness of a point is taken as an absolute value. Then, the smoothness of a line is added. $SMSE_f$ is written as

$$SMSE_f = \sum_{j=3}^{m-2}\left|SN_j\right| \tag{13}$$

where m is the total number of sampled signals.

2.3.3 Filtering algorithm decision criteria

The filter algorithm is established as follows:

$$\text{Restrictions,} \begin{cases} \min\{MSE_f\} \\ \min\{SMSE_f\} \end{cases}. \tag{14}$$

The objective function of filtering algorithm f is defined as:

$$\min\{f\} = \min\{\alpha MSE_f + (1-\alpha)SMSE_f\} \tag{15}$$

where α and $1-\alpha$ are the influencing factors, and the selection weight depends on the specific requirements of signal processing.

3. The proposed method

The flowchart of the proposed method is shown in Fig. 1, and the proposed fault diagnosis method is described as follows:

Step 1. Collect vibration signals under different conditions.

Step 2. Perform EMD decomposition of the original signal to obtain IMF components.

Step 3. Construct a low-pass filter to reduce the noise of the original signal.

Step 4. Perform EMD decomposition on the signal after noise reduction to obtain the IMF components.

Step 5. Perform envelope spectrum analysis on the selected IMF.

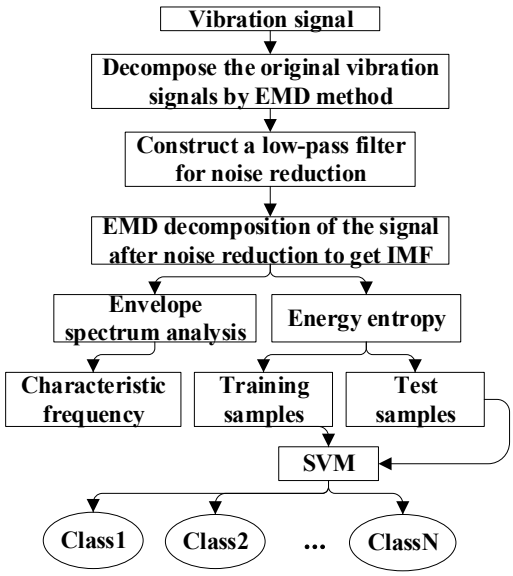

Fig. 1. The flow chart of compound fault diagnosis.

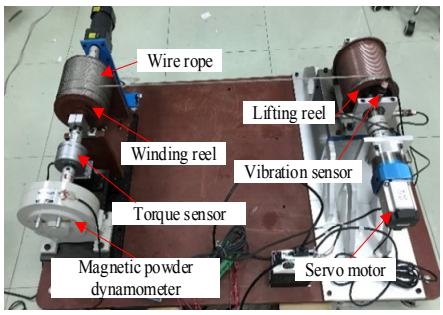

Fig. 2. Compound fault simulation test bench.

Step 6. Extract energy entropy features from IMF, normalize the data, and divide them into training samples and test samples.

Step 7. Train the SVM model and import the test data into the trained classification model for predictive classification.

4. Test bench setup

To carry out fault diagnosis and identification, we built a simulation test bed for the hoist spindle device. The test equipment is shown in Fig. 2.

To develop new fault diagnosis methods, nine operating conditions were designed: (i) normal condition, (ii) bearing outer ring failure, (iii) bearing inner ring failure, (iv) rolling element failure, (v) spindle bending failure, (vi) spindle misalignment failure, (vii) spindle bending and misalignment, (viii) spindle bending and bearing outer ring failure, and (ix) spindle misalignment and bearing inner ring failure. The vibration data under nine working conditions were obtained from the experimental system for feature extraction and recognition.

The test bench was selected from the Panasonic model

Table 1. Specifications of the test bearing.

Feature	Detail
Bearing type	SKF22207CA/W33
Roller diameter/d	8.2 mm
Pitch diameter/D	55 mm
Number of balls/N	30
Contact angle/ θ	0°

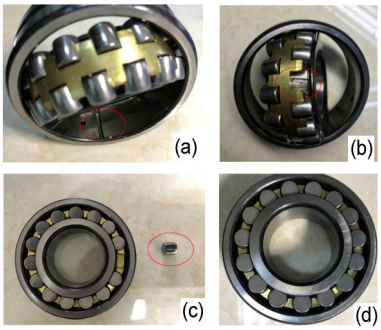

Fig. 3. The object diagram of the roller bearing: (a) outer ring fault; (b) inner ring fault; (c) rolling element fault; (d) normal.

MSMF082L wire type motor; the rated motor speed was 3000 r/min, and the output power was 750 W. The servo motor speed was 20 r/min, and rotational frequency f_r was 0.33 Hz. The sample frequency was 5000 Hz. To simulate the lifting load of the hoist, the magnetic powder dynamometer was used to load the wire rope. The load size was adjusted and displayed by the NX6002 rotational speed and torque measuring instrument. The torque of the dynamometer was adjusted to 20 N·m under different fault states.

5. Experimental settings

5.1 Typical failure test design of rolling bearing of spindle device

The model specifications of the rolling bearings used in the test are shown in Table 1. In this test, linear fault defects were respectively processed on the outer ring, inner ring, and rolling elements of three different bearings. A single point of failure (slit width of 1.5 mm and depth of 1.5 mm) was machined on the outer and inner rings of the bearing by EDM, and a slit was cut longitudinally on the roller by wire cutting. The slit width was 1 mm, and the depth was 1 mm. The faulty bearing is shown in Fig. 3.

The fault characteristic frequencies of the outer ring, inner ring, and rolling element were 4.25 Hz (f_o), 5.745 Hz (f_i), and 1.093 Hz (f_c), which can be calculated by the following formulas [26]:

$$f_o = \frac{N}{2}\left(1-\frac{d}{D}\cos\theta\right)f_r, \tag{16}$$

Table 2. Influence factors, objective function values, and corresponding filtering algorithm.

α and $1-\alpha$	Min{f}	Filtering algorithm
0.1 and 0.9	0.0915	LP4
0.2 and 0.8	0.1743	LP3
0.3 and 0.7	0.2462	LP3
0.4 and 0.6	0.3181	LP3
0.5 and 0.5	0.3899	LP3
0.6 and 0.4	0.4618	LP3
0.7 and 0.3	0.5166	LP2
0.8 and 0.2	0.5622	LP2
0.9 and 0.1	0.5439	LP1

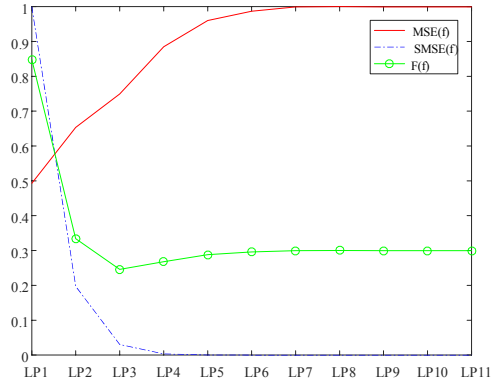

Fig. 4. Curves of MSE, SMSE, and objective functions.

$$f_i = \frac{N}{2}\left(1+\frac{d}{D}\cos\theta\right)f_r, \tag{17}$$

$$f_c = \frac{D}{2d}\left[1-\left(\frac{d}{D}\cos\theta\right)^2\right]f_r. \tag{18}$$

5.1.1 Filtering processing

Taking the outer ring fault as an example, 10240 sampling points were selected as signal analysis data. We abbreviated the following low-pass filter expression:

$$LP3 = IMF_4 + IMF_5 + IMF_6 + IMF_7 + IMF_8 + IMF_9 + IMF_{10} + IMF_{11} + res, \tag{19}$$

$$LP7 = IMF_8 + IMF_9 + IMF_{10} + IMF_{11} + res. \tag{20}$$

For the different influence factors of MSE and SMSE, the minimum value of the objective function was calculated, as shown in Table 2.

According to the analysis of Table 2, in the low-pass filtering algorithms LP1-LP11 with 11 different effects, the objective function value of the algorithm LP3 appeared the most. The effect of the visible algorithm LP3 was stable and optimal. When the value was equal to 0.3, the curves of the MSE, SMSE, and objective functions of the 11 low-pass algorithms LP1-LP11 could be plotted, as shown in Fig. 4.

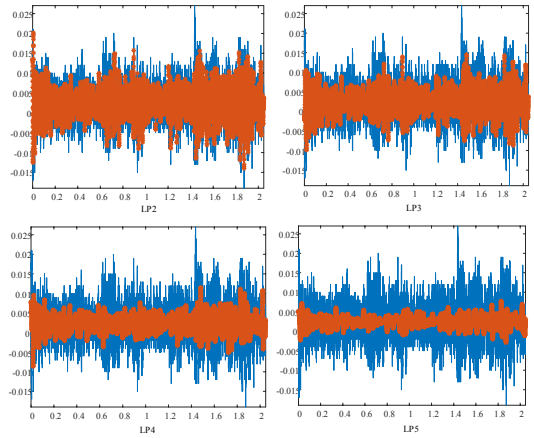

Fig. 5. Noise reduction comparison.

Fig. 4 demonstrates that the objective function obtained a minimum value at LP3. For comparison, we took LP2, LP3, LP4, and LP5 and drew the effect of noise reduction, as shown in Fig. 5. The noise reduction algorithm LP3 was used to reduce the noise of the noisy vibration signal, and the effect was the most optimal.

5.1.2 Hilbert-Huang transform analysis

EMD decomposition was conducted for four kinds of bearing fault signals after noise reduction. We selected the first five IMFs and calculated the correlation between IMF and the original signal according to a cross-correlation pseudo-component determination method [27], as shown in Table 3.

As can be seen from Table 3, the correlation between the IMF1, IMF2, and IMF3 and the original signal was large. Hilbert envelope spectrum analysis was performed on IMF1, IMF2, and IMF3, respectively. Notably, the frequency of the fault signature was easy to extract from the Hilbert envelope spectrum. This spectrum is shown in Figs. 6-8.

Fig. 6 demonstrates that the three envelope spectra of IMF1, IMF2, and IMF3 had peaks at the frequencies of f_o and $2f_o$, which were the failure frequency of the outer ring calculated by the theoretical formula of 4.25 Hz. The three envelope spectra of IMF1, IMF2, and IMF3 in Fig. 7 indicated peaks at frequencies of f_i and $2f_i$, which were the fault frequency of 5.745 Hz calculated by the theoretical formula of the inner circle. As shown in Fig. 8, the three envelope spectra of IMF1, IMF2, and IMF3 had peaks at frequencies f_c and $2f_c$, which were consistent with the fault frequency 1.093 Hz calculated by the theoretical formula.

5.2 Fault test design of main shaft of hoist spindle device

In this work, three kinds of fault tests, namely, typical spindle bending, spindle misalignment, spindle bending, and misalignment, were designed to explore the vibration characteristics of the spindle fault.

The bending failure of the spindle was extruded and bent by

Table 3. The number of interrelationships between the first five orders of IMF and the original signal.

IMF	Outer ring	Inner ring	Rolling element
IMF1	0.4011	0.4999	0.4606
IMF2	0.5397	0.4567	0.5680
IMF3	0.4093	0.4150	0.3902
IMF4	0.3814	0.3882	0.3823
IMF5	0.3730	0.3441	0.2665

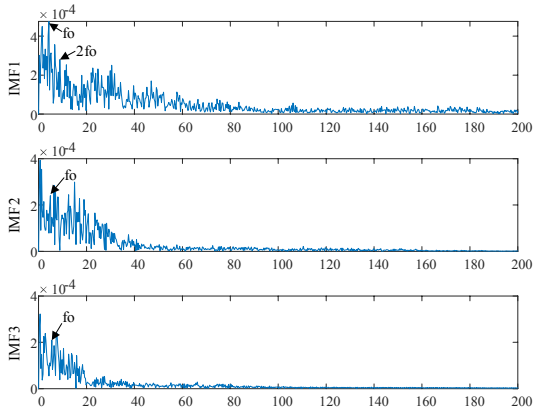

Fig. 6. Envelope spectrum of outer ring.

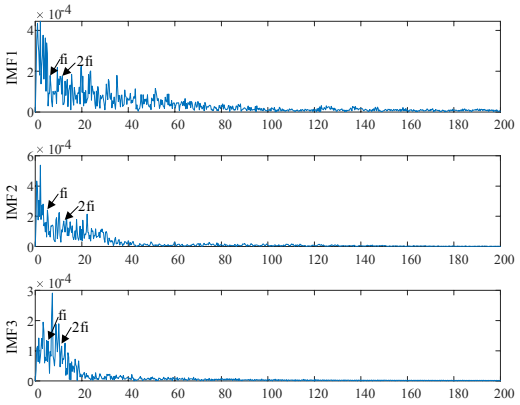

Fig. 7. Envelope spectrum of inner ring.

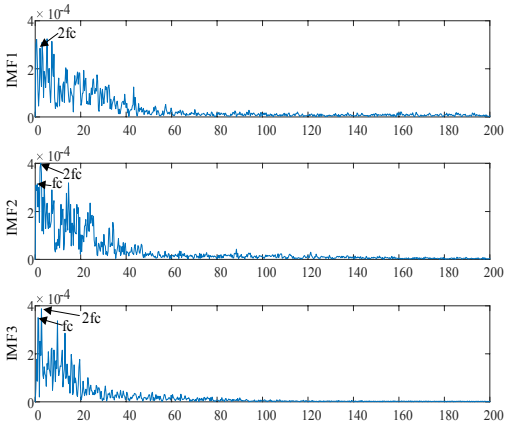

Fig. 8. Envelope spectrum of rolling element.

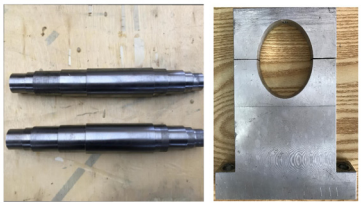

(a) (b)

Fig. 9. (a) Bending spindle; (b) faulty bearing housing.

pressing. The overall bending degree of the spindle was approximately 0.8 mm, as shown in Fig. 9(a). The bearing housing was made of aluminum alloy. The faulty bearing housing is shown in Fig. 9(b). The center of the mass position of the bearing hole of the fault bearing housing was 1.5 mm lower than that of the normal bearing housing. This size allows the simulation of the misalignment of the spindle caused by the deformation of the bearing housing.

The compound failure in this section presents the two failure forms of spindle bending and spindle imbalance in the same group of experiments at the same time. During the test, the normal spindle was replaced with the bending spindle, and the normal bearing block was replaced away from the servo motor end with the fault bearing block.

The Hilbert envelope spectrum of the first three signals is presented across Figs. 10-16. For comparison, Hilbert envelope demodulation was performed on the first three order IMFs of the normal spindle signal, and Hilbert envelope spectrum is shown in Fig. 11.

Fig. 10 shows that the Hilbert envelope spectrum of the spindle bending signal had a peak at the fundamental frequencies of 13.12 Hz, 12.21 Hz, and 12.51 Hz and at the double frequency of 25.02 Hz and 24.11 Hz. By comparing the envelope spectrum of the IMF of the normal bearing, the fundamental frequency and double frequency of characteristic frequency did not appear in the Hilbert envelope spectrum of the IMF of the normal bearing signal. Therefore, we can approximately believe that the characteristic frequency f_b caused by spindle bending failure was approximately 12.5 Hz. The Hilbert envelope spectrum of the IMF of the misalignment signal in Fig. 13 shows that peaks appeared at frequencies of 7.935 Hz and 7.629 Hz. In addition, peaks appeared at the double frequencies of 14.34 Hz, 14.95 Hz, and 15.26 Hz. By comparison with Fig. 11, we can approximately assume that the characteristic frequency f_m caused by the misalignment fault of the spindle was approximately 7.6 Hz.

From the envelope spectrum of the composite signal shown in Fig. 15, we found that the peak value appeared at 12.21 Hz, 12.82 Hz, and 13.12 Hz and at the double frequency of 24.41 Hz and 24.72 Hz. This outcome was consistent with the fault characteristic frequency of the bending fault. A peak also appeared at 7.019 Hz and 7.629 Hz in the envelope spectrum and at the double frequency of 14.34 Hz and 14.95 Hz. This frequency component was consistent with the frequency of the fault characteristic caused by the misalignment of the spindle.

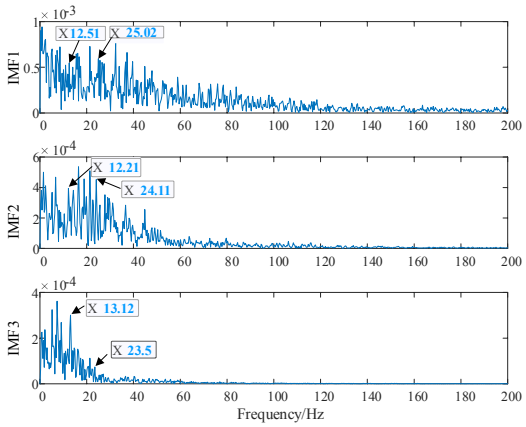

Fig. 10. The envelope spectrum of bending fault.

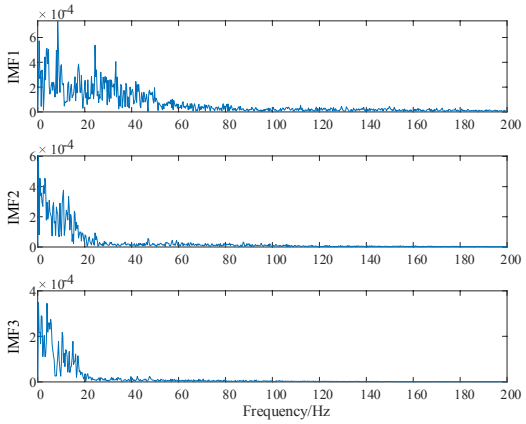

Fig. 11. The envelope spectrum of normal signal.

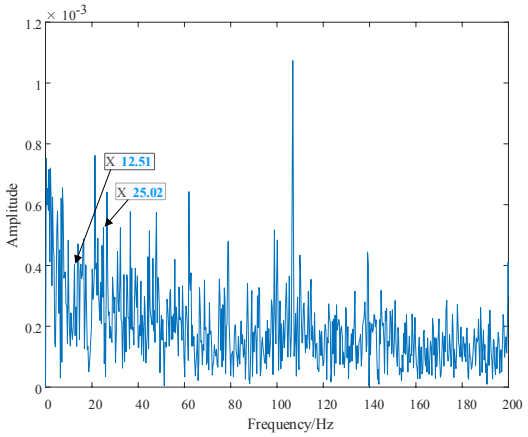

Fig. 12. The original signal envelope spectrum of the bending fault.

To verify the correctness of the characteristic frequencies extracted from the IMF envelope spectrum further, we directly performed Hilbert envelope demodulation for the three signals to obtain the Hilbert envelope spectrum of fault signals. In the envelope spectrum of Fig. 12, the peak value was observed at the fundamental frequency of 12.51 Hz, and the peak value also appeared at the double frequency of 25.02 Hz. In Fig. 14,

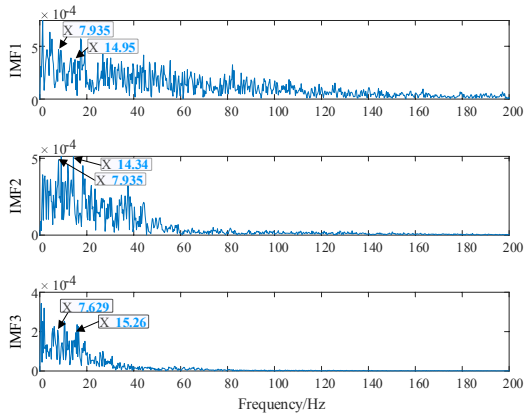

Fig. 13. The envelope spectrum of the misalignment fault.

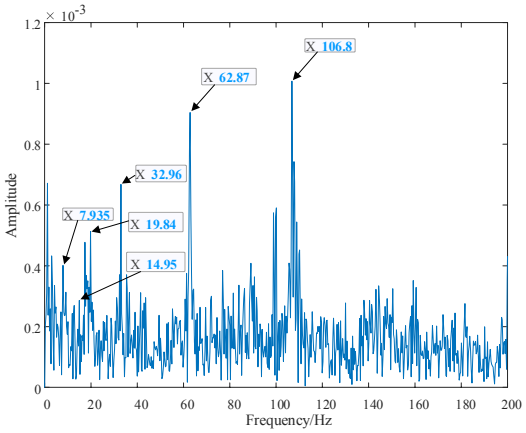

Fig. 14. The original signal envelope spectrum of the misalignment fault.

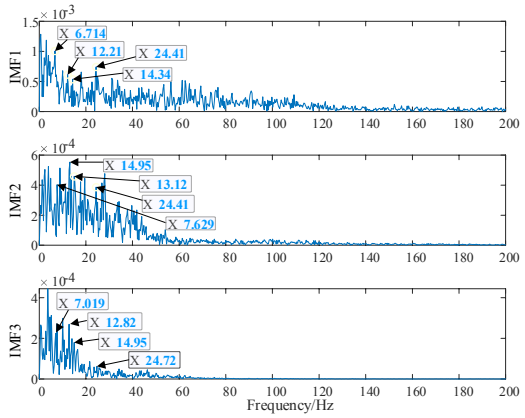

Fig. 15. The envelope spectrum of the spindle composite fault.

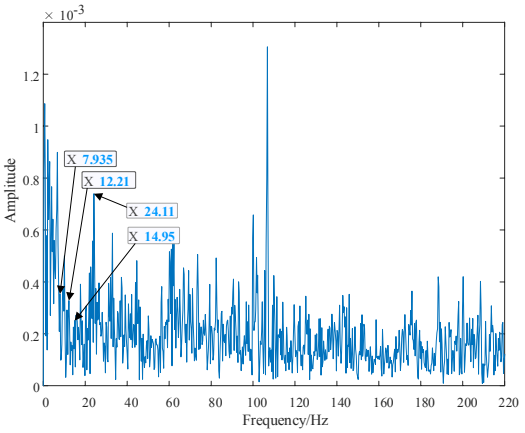

Fig. 16. The envelope spectrum of the spindle composite fault original signal.

the envelope spectrum had an evident peak value at 7.935 Hz, and the peak value also occurred at the multifold frequency of 14.95 Hz, 19.84 Hz, and 32.96 Hz. From the envelope spectrum of the complex signal in Fig. 16, we also found the peak value at 7.935 Hz and 12.21 Hz and the double frequency of 14.95 Hz and 24.11 Hz.

Therefore, the fault frequency extracted from the IMF decomposed by EMD was consistent with the characteristic frequency observed in the Hilbert envelope spectrum directly obtained from the fault signal. This outcome further verified the accuracy of the fault frequency extracted from the main shaft fault signal by the EMD method.

In most cases, by comparing the features of the corresponding parts of the normal signal, the new frequency components can be approximately considered as the fault characteristic frequency.

5.3 Design of composite failure test for hoist spindle device

According to the actual working conditions, this section designs two kinds of composite fault tests of the spindle bending and bearing outer ring (compound one) and the spindle misalignment and bearing inner ring (compound two).

IMF1, IMF2, and IMF3 were selected for envelope spectrum analysis, as shown in Figs. 17 and 18.

From the envelope spectrum of IMF1 shown in Fig. 17, we can find evident peaks at 4.578 Hz and 4.883 Hz in the envelope spectrum and double frequency of 9.46 Hz and 10.38 Hz. These frequencies were close to the theoretical characteristic frequency of 4.25 Hz of the outer ring fault of the rolling bearing, which could be considered the frequency component caused by the outer ring fault of the rolling bearing. Peaks also appeared at 11.9 Hz, 12.21 Hz, and 12.82 Hz and the double frequency of 23.8 Hz, 25.33 Hz, and 25.63 Hz. These frequencies were close to the fault characteristic frequency of the spindle bending fault of 12.5 Hz. Hence, they can be considered the fault frequency components generated by the spindle bending fault.

In the envelope spectrum shown in Fig. 18, peak values were found at 7.019 Hz, 7.324 Hz, and 7.629 Hz, which were close to the fundamental frequency of the fault characteristic frequency of the spindle misalignment fault. Moreover, the two instances of the frequency component of 14.34 Hz appeared in the envelope spectrum, which was consistent with the misalignment of the spindle.

Peaks also appeared at 5.188 Hz and 5.798 Hz in the envelope spectrum, which could be considered the frequency component caused by the inner ring fault.

Therefore, the EMD decomposition was highly effective in extracting the characteristic frequency of the faulty center of the spindle and the characteristic frequency of the fault of the inner ring of the bearing.

To verify the extracted fault frequency components further, the relevant IMFs were selected on the basis of the kurtosis principle to reconstruct the signals; then, the reconstructed signals were analyzed [28]. For the IMF decomposed by EMD, we only selected the first five IMF and calculated their kurtosis, as shown in Table 4. As the table presents, the kurtosis values of IMF1, IMF2, and IMF3 were larger and greater than 3.

Table 4. The kurtosis of the IMF.

IMF	Compound one	Compound two
IMF1	4.5634	4.5634
IMF2	3.3574	3.4010
IMF3	3.2622	3.0030
IMF4	3.1128	2.8156
IMF5	2.7694	2.7990

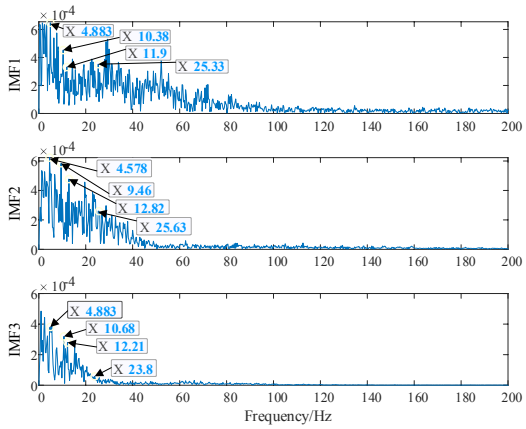

Fig. 17. The envelope spectrum of compound one.

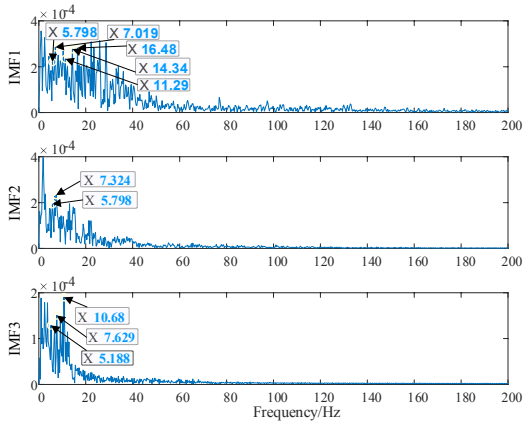

Fig. 18. The envelope spectrum of compound two.

Therefore, the first three IMFs could be selected for reconstruction signals, and Hilbert envelope spectrum analysis could be performed on the reconstructed signals, as shown in Figs. 19 and 20.

Fig. 19 reveals that the Hilbert envelope spectrum of reconstructed signals showed clear peak values at 4.883 Hz and double frequency of 9.46 Hz, which were close to the characteristic frequency of bearing outer ring fault. These frequencies could be considered the failure frequency of the bearing outer ring. Moreover, the peak value could be observed at 13.73 Hz, which were close to the fault characteristic frequency of spindle bending at 12.5 Hz. This observation indicated that the reconstruction signal could show the fault characteristic frequency of spindle bending.

In the Hilbert envelope spectrum of the reconstructed signal in Fig. 20, the peak occurred at 6.104 Hz and the double frequency of 10.07 Hz, which was close to the fault characteristic frequency of the inner ring of the bearing. Moreover, peaks appeared at 7.019 Hz and 14.95 Hz, which could be considered the characteristic frequency of the misalignment fault. The accuracy and reliability of extracting fault feature frequencies

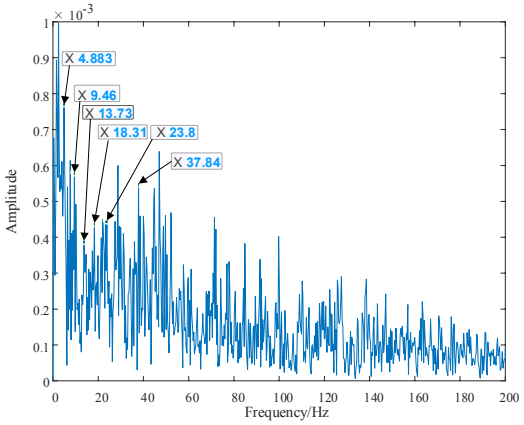

Fig. 19. Hilbert envelope spectrum of the compound one reconstructed signal.

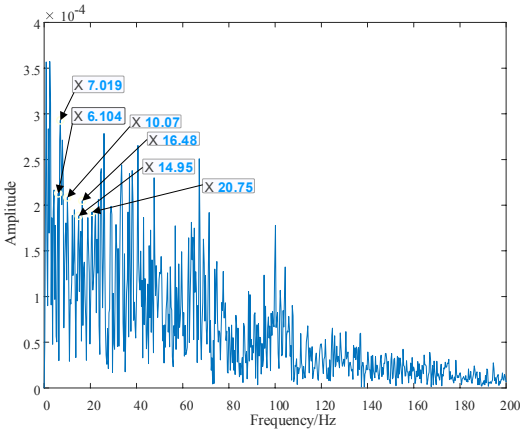

Fig. 20. Hilbert envelope spectrum of the compound two reconstructed signal.

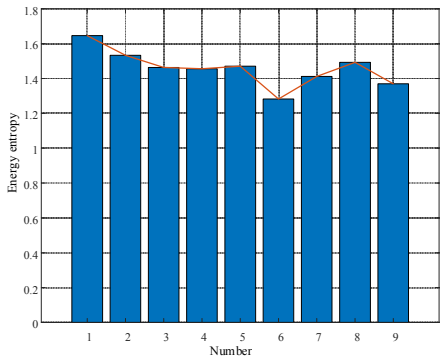

Fig. 21. The curve of energy entropy under different states.

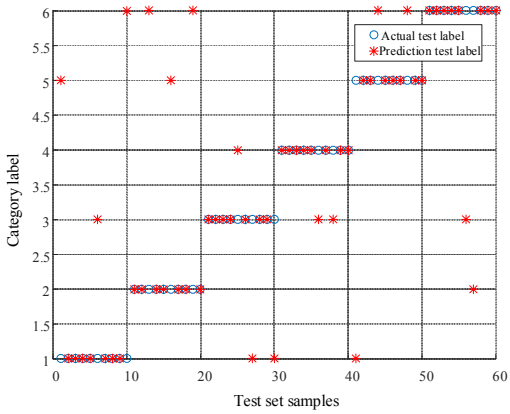

Fig. 22. Test classification results.

by EMD were also verified.

The characteristic frequencies observed in the envelope spectrum of reconstructed signals were basically consistent with those observed in the Hilbert envelope spectrum of IMF, which further verified the accuracy and reliability of extracting fault characteristic frequencies using EMD.

5.4 Study on fault identification of spindle device based on intrinsic mode energy entropy and SVM

From the previous fault data samples, 40 groups of data segments were randomly selected for each fault sample, with a length of 2048 points. According to the formula, we calculated the energy entropy for the first five IMFs of each group of signals. The average value of energy entropy in different fault states is shown in Fig. 21.

The first three IMF energy entropy values of normal signal, inner ring fault signal, outer ring fault signal, rolling element fault signal, compound one fault signal, and compound two fault signal were selected, respectively, to form the feature vector.

For the six states, 30 sets of data were selected as training samples for each state, and the remaining 60 sets of data were used as test samples. The training samples were input into SVM for training. Furthermore, radial basis function (RBF) and the cross-validation search algorithm were used in the model.

Then, 60 groups of test sample data were input into the model for fault prediction and classification. The test results are shown in Fig. 22, where 1 represents the normal state, 2 represents the inner ring fault, 3 represents the outer ring fault, 4 represents the rolling body fault, 5 represents the compound one fault, and 6 represents the compound two fault. The accuracy rate is 73.3 % (44/60).

6. Conclusion

On the basis of the above fault simulation test and data analysis, the following conclusions are obtained:

1) By decomposing the original vibration signals to obtain IMF, as well as selecting and combining them, different low-pass filtering algorithms can be constructed. By balancing MSE and SMSE and selecting the influencing factors, the optimal filtering algorithm can be determined. The improved algorithm is composed of the remaining modal components and the residual after removing the first three modal components.

2) To solve the problem that fault vibration information is difficult to demodulate, EMD method and envelope spectrum analysis are applied to the fault diagnosis of the hoist spindle device. Applying the EMD method and envelope spectrum analysis to the fault diagnosis of the hoist spindle device can effectively demodulate the fault vibration information. The IMF components are obtained by decomposing the signal after noise reduction. In addition, the first three IMF components with large correlation coefficients are selected for envelope spectrum analysis, which can effectively extract the fault characteristic frequency.

3) The energy entropy values of signals under different fault states are evidently different from the energy entropy values of normal signals. Using the energy entropy value as the feature vector, combined with the SVM method, can effectively identify the working state of the spindle device.

This study can provide an important reference for the fault diagnosis of the spindle device of the hoist. Moreover, our findings have certain practicability in the field.

Acknowledgments

The authors thanked all those who helped them in writing this thesis. The research was supported by the National Key Research and Development Program (2017YFF0210604), the National Natural Science Foundation of China (No.51975572), the Top-notch Academic Programs Project of Jiangsu Higher Education Institutions (TAPP), the Project funded by the Priority Academic Program Development of Jiangsu Higher Education Institutions (PAPD).

References

[1] J. L. Li, S. Jiang, M. H. Li and J. C. Xie, A fault diagnosis method of mine hoist disc brake system based on machine

learning, *Applied Sciences*, 10 (5) (2020) 1768.
[2] C. Tang, G. Zhou, Z. Gao, X. Shu and P. Chen, A novel rail inspection robot and fault detection method for the coal mine hoisting system, *Intelligent Transportation Systems Magazine IEEE*, 11 (2) (2019) 110-121.
[3] X. J. Chen, Y. M. Yang, Z. X. Cui and J. Shen, Vibration fault diagnosis of wind turbines based on variational mode decomposition and energy entropy, *Energy*, 174 (2019) 1100-1109.
[4] H. K. Li, Z. X. Zhang, Z. G. Guo, S. Zou and F. T. Wang, Rolling bearing fault diagnosis using Hough transform of time-frequency image, *Journal of Vibration, Measurement and Diagnosis,* 30 (6) (2010) 634-637.
[5] W. Bartelmus and R. Zimroz, A new feature for monitoring the condition of gear boxes in non-stationary operating conditions, *Mechanical Systems and Signal Processing*, 23 (5) (2009) 1528-1534.
[6] W. Zeng, J. Yuan, C. Yuan, Q. Wang and Y. Wang, A new approach for the detection of abnormal heart sound signals using TQWT, VMD and neural networks, *Artificial Intelligence Review*, 6 (54) (2020) 1613-1647.
[7] V. K. Rai and A. R. Mohanty, Bearing fault diagnosis using FFT of intrinsic mode functions in Hilbert-Huang transform, *Mechanical Systems and Signal Processing*, 21 (6) (2007) 2607-2615.
[8] P. Tse, W. X. Yang and H. Y. Tam, Machine fault diagnosis through an effective exact wavelet analysis, *Journal of Sound and Vibration*, 277 (2004) 1005-1024.
[9] N. E. Huang et al., The empirical mode decomposition and the Hilbert spectrum for nonlinear and non-stationary time series analysis, *Proceedings of the Royal Society*, 454 (1998) 903-995.
[10] Y. G. Lei, Z. J. He and Y. Y. Zi, EEMD method and WNN for fault diagnosis of locomotive roller bearings, *Expert Systems with Applications*, 38 (6) (2011) 7334-7341.
[11] P. M. Shi, S. J. An, P. Li and D. Y. Han, Signal feature extraction based on cascaded multi-stable stochastic resonance denoising and EMD method, *Measurement*, 90 (2016) 318-328.
[12] F. T. Wang, C. X. Liu, W. S. Su, Z. G. Xue, Q. K. Han and H. K. Li, Combined failure diagnosis of slewing bearings based on MCKD-CEEMD-CEEMD-ApEn, *Shock and Vibration*, 2018 (2018) 1-13.
[13] A. B. Ming, W. Zhang, Z. Y. Qin and F. L. Chu, Envelope calculation of the multi-component signal and its application to the deterministic component cancellation in bearing fault diagnosis, *Mechanical Systems and Signal Processing*, 50-51 (2015) 70-100.
[14] Y. G. Lei, J. Lin, Z. J. He and M. J. Zuo, A review on empirical mode decomposition in fault diagnosis of rotating machinery, *Mechanical Systems and Signal Processing*, 35 (1-2) (2013) 108-126.
[15] C. Cortes and V. Vapnik, Support vector networks, *Machine Learning*, 20 (3) (1995) 273-297.
[16] Y. Fan, C. Zhang, Y. Xue, J. Wang and F. Gu, A bearing fault diagnosis using a support vector machine optimised by the self-regulating particle swarm, *Shock and Vibration*, 2020 (5) (2020) 1-11.
[17] J. Q. Zhang, J. Zhang, M. Zhong, J. D. Zheng and L. G. Yao, A GOA-MSVM based strategy to achieve high fault identification accuracy for rotating machinery under different load conditions, *Measurement*, 163 (2020) 108067.
[18] Y. J. Niu, J. Y. Fei, Y. Y. Li and D. Wu, A novel fault diagnosis method based on EMD, cyclostationary, SK and TPTSR, *Journal of Mechanical Science and Technology*, 34 (5) (2020) 1925-1935.
[19] D. Y. Han, N. Zhao and P. M. Shi, Gear fault feature extraction and diagnosis method under different load excitation based on EMD, PSO-SVM and fractal box dimension, *Journal of Mechanical Science and Technology*, 33 (2) (2019) 487-494.
[20] T. Guo and Z. M. Deng, An improved EMD method based on the multi-objective optimization and its application to fault feature extraction of rolling bearing, *Applied Acoustics*, 127 (2017) 46-62.
[21] M. C. Pan and W. C. Tsao, Using appropriate IMFs for envelope analysis in multiple fault diagnosis of ball bearings, *International Journal of Mechanical Sciences*, 69 (2013) 114-124.
[22] Z. L. Mou, X. B. Niu and C. Wang, A precise feature extraction method for shock wave signal with improved CEEMD-HHT, *Journal of Ambient Intelligence and Humanized Computing*, 2020 (3) (2020).
[23] J. B. Ali, N. Fnaiech, L. Saidi, B. C. Morello and F. Fnaiech, Application of empirical mode decomposition and artificial neural network for automatic bearing fault diagnosis based on vibration signals, *Applied Acoustics*, 89 (2015) 16-27.
[24] Y. Yu, D. J. Yu and J. S. Cheng, A roller bearing fault diagnosis method based on EMD energy entropy and ANN, *Journal of Sound and Vibration*, 294 (1-2) (2006) 269-277.
[25] Y. Zheng, J. Yue, X. F. Sun and J. Chen, Studies of filtering effect on internal solitary wave flow field data in the South China Sea using EMD, *Advanced Materials Research*, 518-523 (2012) 1422-1425.
[26] V. K. Rai and A. R. Mohanty, Bearing fault diagnosis using FFT of intrinsic mode functions in Hilbert-Huang transform, *Mechanical Systems and Signal Processing*, 21 (6) (2007) 2607-2615.
[27] W. S. Su, F. T. Wang, Z. X. Zhang, Z. G. Guo and H. K. Li, Application of EMD denoising and spectral kurtosis in early fault diagnosis of rolling element bearings, *Journal of Vibration and Shock,* 22 (1) (2010) 3537-3540.
[28] H. Li, T. Liu, X. Wu and Q. Chen, Research on bearing fault feature extraction based on singular value decomposition and optimized frequency band entropy, *Mechanical Systems and Signal Processing*, 118 (2019) 477-502.

Jun Gu is currently pursuing the Doctorate degree in Mechatronic Engineering in China University of Mining and Technology, Xuzhou, China. His current research interests include fault diagnosis and monitoring, signal processing.